Binding of heparan sulfate to human cystatin C modulates inhibition of cathepsin L: Putative consequences in mucopolysaccharidosis

Sophie Denamur, Thibault Chazeirat, Martyna Maszota-Zieleniak, Romain Vivès, Ahlame Saidi, Fuming Zhang, Robert J. Linhardt, François Labarthe, Sergey A. Samsonov, Gilles Lalmanach, et al.

Carbohydrate Polymers 293 (2022) 119734

Contents lists available at ScienceDirect

Carbohydrate Polymers

journal homepage: www.elsevier.com/locate/carbpol

Binding of heparan sulfate to human cystatin C modulates inhibition of cathepsin L: Putative consequences in mucopolysaccharidosis

Sophie Denamur [a,b,c,1], Thibault Chazeirat [a,b,1], Martyna Maszota-Zieleniak [d], Romain R. Vivès [e], Ahlame Saidi [a,b], Fuming Zhang [f], Robert J. Linhardt [f], François Labarthe [c,g], Sergey A. Samsonov [d], Gilles Lalmanach [a,b], Fabien Lecaille [a,b,*]

[a] University Tours, Tours, France
[b] INSERM, UMR 1100, Centre d'Etude des Pathologies Respiratoires (CEPR), Team "Mécanismes protéolytiques dans l'inflammation", Tours, France
[c] Pediatric Department, Reference Center for Inborn Errors of Metabolism ToTeM, CHRU Tours, France
[d] Faculty of Chemistry, University of Gdańsk, Poland
[e] University Grenoble Alpes, CNRS, CEA, IBS, Grenoble, France
[f] Center for Biotechnology and Interdisciplinary Studies, Rensselaer Polytechnic Institute, Troy, NY, USA.
[g] INSERM, UMR 1069, Nutrition, Croissance et Cancer (N2C), Tours, France.

ARTICLE INFO

Keywords:
Glycosaminoglycan
Inhibitor
Lung
Molecular dynamic
Protease

ABSTRACT

Mucopolysaccharidoses (MPS) are a group of rare lysosomal storage diseases characterized by glycosaminoglycan (GAG) accumulation causing progressive multi-organs dysfunction and ultimately severe cardio-respiratory damages. Human cystatin C (hCC), a potent inhibitor of cysteine cathepsins, plays an important role in respiratory diseases. However, its regulation remained unknown in MPS. Herein, elevated hCC levels were measured in respiratory specimens from MPS-I, -II, and -III patients and were significantly correlated with severe respiratory symptoms (rs = 0.7173). Heparan sulfate (HS), a prominent GAG, dampened its inhibitory activity toward cathepsin L in a dose-dependent manner. HS and HS-oligosaccharides bound tightly hCC, in combination with a secondary structure rearrangement. Molecular modeling studies identified three HS binding regions in hCC, including the N-terminus, which is crucial in the inhibition of cathepsins. Impairment of inhibitory potential of hCC may reflect abnormal regulation of proteolytic activity of cathepsin L in lung, ultimately contributing to the severity of MPS.

1. Introduction

Mucopolysaccharidoses (MPS, seven types listed) are rare metabolic diseases associated to a lysosomal enzyme deficiency, which leads to an abnormal accumulation of glycosaminoglycans (GAGs) that compromises proper cell function (Muenzer, 2011). Multiple progressive symptoms in MPS patients are observed, including neurological, skeletal, cardiac, and respiratory dysfunctions. The prognosis of the disease outcome is variable depending on the organs affected and can induce premature death following cardio-pulmonary alterations (Berger et al., 2013; Zhou et al., 2020). Even if palliative treatments can be proposed for all types of MPS, most of current therapies are not curative, but partly improve some symptoms of the disease. Therefore, conducting research to address unmet medical needs is required. In this regard, cellular and molecular mechanisms underlying this pathology remain largely unknown, notably the status and regulation of the protease-antiprotease

Abbreviations: AMC, 7 amido-4-methylcoumarin; Cathepsin L, Cat L; CS, chondroitin sulfate; DS, dermatan sulfate; DTT, dithiothreitol; GAG, glycosaminoglycan; GlcA, glucuronic acid; GlcNAc, *N*-acetyl-D-glucosamine; GlcNS, *N*-sulfoglucosamine; GlcNS(6S), GlcNS 6-sulfate, α-L-iduronidase; GRSS, global respiratory symptoms severity; Hep, heparin; HS, heparan sulfate, α-L-iduronidase; IdoA, iduronic acid; IdoA(2S), IdoA 2-sulfate; KS, keratan sulfate; MD, molecular dynamics; MMP, matrix metallo-proteinase; MPS, mucopolysaccharidosis; Z, benzyloxycarbonyl.

* Corresponding author at: Université de Tours, INSERM, UMR 1100, CEPR, 10 Boulevard Tonnellé, F-37032 Tours cedex, France.
E-mail addresses: sophie.denamur@univ-tours.fr (S. Denamur), thibault.chazeirat@etu.univ-tours.fr (T. Chazeirat), romain.vives@ibs.fr (R.R. Vivès), ahlame.saidi@univ-tours.fr (A. Saidi), zhangf2@rpi.edu (F. Zhang), linhar@rpi.edu (R.J. Linhardt), francois.labarthe@univ-tours.fr (F. Labarthe), sergey.samsonov@ug.edu.pl (S.A. Samsonov), gilles.lalmanach@univ-tours.fr (G. Lalmanach), fabien.lecaille@univ-tours.fr (F. Lecaille).
[1] Equal contribution.

https://doi.org/10.1016/j.carbpol.2022.119734
Received 20 April 2022; Received in revised form 30 May 2022; Accepted 11 June 2022
Available online 18 June 2022

balance, which is necessary to maintain the integrity of tissues/organs. In a recent study, we reported that the overall endopeptidase activity of human cysteine cathepsins (*i.e.* family C1, subfamily C1A of cysteine proteases) was significantly reduced in respiratory secretions of MPS-I, -II and -III patients and correlated negatively to the severity of respiratory symptoms (Chazeirat et al., 2021). In addition, we demonstrated that heparan sulfate (HS), the most prominent GAG accumulated in MPS type I, II, and III, inactivated specifically cathepsin V, which is a potent elastolytic protease implicated in extracellular matrix remodeling. In addition, current evidence suggests that proteolytic activity of cysteine cathepsins is specifically modulated by GAGs, based on their concentration, sulfation pattern and the difference of repeating disaccharide units comprising GAGs (for review: Novinec et al., 2014). Otherwise, abnormal expression and/or activity of both lysosomal and extra-lysosomal cathepsins B, H, L, C, K, and S have been found to correlate with major clinical symptoms such as neurological, cardiac, and skeletal disorders in MPS (for review: De Pasquale et al., 2020).

Under physiological conditions, cysteine cathepsins are tightly regulated by their endogenous inhibitors of the cystatin family (family I25, clan IH), which includes stefins (type 1), cystatins (type 2), and kininogens (type 3) (Lalmanach et al., 2021, 2015). Human cystatin C (hCC), a low-molecular-weight basic protein (120 residues, ~13 kDa, isoelectric point: pI = 9.3) expressed and secreted by a broad variety of human cells and tissues, is the best well-characterized member of the type 2 cystatin family (Abrahamson et al., 2003). Extracellular hCC, which is ubiquitously found in body fluids, is the major extracellular cysteine cathepsins inhibitor and the most potent tight-binding inhibitor of cysteine cathepsins (Abrahamson, 1994; Abrahamson et al., 1986; Lecaille et al., 2008; Turk et al., 2008). An imbalance of protease/anti-protease in favor of proteolysis is found in inflammatory disorders such as rheumatoid arthritis, osteoporosis, bone cancers, but also in lung diseases including cystic fibrosis, chronic obstructive pulmonary disease, emphysema, or asthma (Kasabova et al., 2011). Alternatively, a deficit or inactivation of cathepsins and/or a hCC increased level could be associated with cases of idiopathic pulmonary fibrosis (IPF) or alveolar proteinosis (Bühling et al., 2004; Kasabova, Joulin-Giet, Lecaille, Saidi, et al., 2014; Lalmanach et al., 2006). Interestingly, hCC has been proposed as a prognostic marker in IPF patients, due to its high level in the bronchoalveolar lavage fluids of patients, regardless of IPF grades (Kasabova et al., 2016; Kasabova, Joulin-Giet, Lecaille, Saidi, et al., 2014).

2. Hypotheses

This led us to determine whether hCC could be specifically overexpressed in respiratory secretions of MPS patients, raising the question of its potential use as a specific biomarker of respiratory symptoms severity during MPS. Furthermore, previous studies reported that the potency of distinct protease inhibitors such as serpins (*i.e.*, anti-thrombin III, α1-proteinase inhibitor, kallistatin) and tissue inhibitor metalloprotease-3 (TIMP-3) can be enhanced by the presence of GAGs (Higgins et al., 2010; Rein et al., 2011; Ruiz-Gómez et al., 2019). A recent report indicated that the mouse ortholog cystatin C (70.8 % of identity with hCC) binds to HS in a pH-dependent manner, impairing papain inhibition, the vegetal archetype of cysteine cathepsins (Zhang et al., 2021). Therefore, potential interactions of GAGs with hCC were investigated, to assess whether elevated GAGs levels, in particular HS, may modulate the inhibitory potential of hCC. Here, we quantified the expression level of hCC in MPS-I, -II, and -III patients and considered its clinical significance in the early diagnosis of global respiratory symptoms. In conjunction, the binding mode between HS and hCC was deciphered (equilibrium binding constant, structural motifs involved) and the consequences of this binding on cathepsin L inhibition were characterized *in vitro*. Additionally, molecular docking and dynamic simulations studies provided structural insights into the interactions between hCC and HS oligosaccharides. This study sheds light on how the inhibitory potential of hCC is finely tuned by HS, which in turn may reflect an abnormal regulation of lung cathepsins and ultimately contribute to the severity of MPS.

3. Materials and methods

3.1. Ethical statement, patient status and clinical specimens

This study was approved by the French National bioethical authorities (n°ID-RCB: 2019-A01361-56). Respiratory specimens, including sputum and tracheal aspirates were collected from MPS patients (N = 11, with 2 MPS-I, 5 MPS-II, and 4 MPS-III) and non-MPS patients (N = 9). Clinical features of patients included in the study, sample collection, processing, total protein quantification of cell-free supernatants of sputum and tracheal aspirates and storage were detailed in a previous report (Chazeirat et al., 2021). A global respiratory symptoms severity (GRSS) score was given for each patient according to four types of symptoms: ear-nose-throat symptoms, pulmonary symptoms, clinical symptoms of obstructive sleep apnea, and skeletal abnormalities causing restrictive lung disease. The GRSS score was graduated from 0 to 4, according to the number of respiratory complications for each patient (Chazeirat et al., 2021). Serum creatinine concentration was measured using the Roche enzymatic creatinine assay (F. Hoffmann-La Roche, Basel, Switzerland), as reported elsewhere (Hoste et al., 2014). Clearance was calculated using the Schwartz method (Schwartz & Work, 2009).

3.2. Immunohistochemical analysis of cystatin C in a MPS-I lung biopsy

Lung sections (obtained from a post-mortem 2-year-old female with MPS-I) were formalin fixed and paraffin embedded (Gupta et al., 2013). Detection of cystatin C was performed without antigen retrieval after removing paraffin with xylene. Tissue sections were rehydrated by sequential washings with ethanol and water. The endogenous peroxidase activity was blocked by incubating sections in 3 % H_2O_2 solution for 20 min. Non-specific binding sites were blocked with 5 % bovine serum albumin (BSA) in phosphate buffered saline, pH 7.4 (PBS) for 1 h at room temperature. Sections were then incubated overnight at 4 °C with mouse anti-cystatin C (1:400 dilution in PBS with 5 % BSA, R&D Systems). The slides were washed and further incubated with peroxidase-conjugated mouse anti-goat IgG (1:1000, R&D Systems) for 1 h. Peroxidase activity in tissue sections was visualized using 3, 3′-diaminobenzidine as a substrate solution. Lung sections were counter-stained with Gill's hematoxylin for 1 min, dehydrated, cleared in xylene, and mounted in Vectamount permanent medium (Vector Labs, Peterborough, U.K.).

3.3. Quantification of hCC and glycosaminoglycans in respiratory specimens

Following electrophoretic running of non-MPS and MPS cell-free supernatants (375 μg of total protein/well; 4–20 % SDS-PAGE, Bio-Rad, Mini Protean TGX, Marnes-la-Coquette, France) under reducing conditions, hCC was immunodetected by a mouse anti-cystatin C primary antibody (1:1000 in PBS milk 5 %) incubated overnight at 4 °C. Horseradish peroxidase (HRP)-anti-IgG antibody conjugate (1:5000 PBS milk 5 %) was incubated for 1 h at room temperature, and immunoreactive bands were visualized using an enhanced chemiluminescence assay kit (ECL Plus Western blotting detection system; Amersham Biosciences, UK). Alternatively, quantitative analysis of cystatin C was performed with a sandwich ELISA Duoset kit (R&D Systems). Each sample was run in triplicate. Total amount of sulfated GAGs, chondroitin sulfate (CS), dermatan sulfate (DS), and HS levels were previously measured as reported elsewhere (Chazeirat et al., 2021). Data were reported as median ± interquartile.

3.4. Enzymes, reagents, and chemicals

Recombinant human cathepsin L and benzyloxycarbonyl-Phe-Arg-7-amino-4-methyl coumarin (Z-Phe-Arg-AMC) were from R&D Systems (Minneapolis, USA). Active site titration of cathepsin L was performed using the titrating agent, trans-epoxysuccinyl-L-leucylamido(4-guanidino)butane (E-64), an irreversible inhibitor of cysteine proteases (Sigma-Aldrich, Saint-Quentin Fallavier, France) according to the method described elsewhere (Barrett et al., 1982). Heparinases I, II, III, Δ-4,5-glycuronidase, and chondroitinase B, all from *Flavobacterium heparinum* were purchased from Grampenz (Upper Ardoe, Aberdeen, Scotland). Dnase I from bovine pancreas was purchased from Sigma-Aldrich. Pepstatin A, EDTA, 4-(2-aminoethyl) benzenesulfonyl fluoride hydrochloride (AEBSF, Pefabloc), *S*-methyl thiomethanesulfonate (MMTS) were obtained from Sigma-Aldrich (Saint Quentin Fallavier, France). Recombinant hCC was purchased from HyTest Ltd. (Turku, Finland). Chondroitin 4-sulfate (C4-S) from bovine trachea (20–30 kDa), chondroitin 6-sulfate (C6-S) from shark cartilage (~63 kDa), dermatan sulfate (DS) from porcine intestinal mucosa (~14 kDa), and heparin (Hep) from porcine intestinal mucosa (15–17 kDa) were from Sigma-Aldrich. Heparan sulfate (HS) from porcine intestinal mucosa (~15 kDa, batch number HI-11098) was from Celsus Laboratories (Cincinnati, Ohio, USA). HS di- (HS dp2) and tetrasaccharide (HS dp4) were prepared from controlled partial heparinase treatment of commercial porcine intestine heparan sulfate (Celsus Laboratories) followed by size fractionation using Sephadex G-50 column (Sigma-Aldrich), as reported elsewhere (Hileman et al., 1997).

3.5. Enzymatic activity of exogenous cathepsin L in respiratory specimens

According to quantification of cystatin C by ELISA, cell-free supernatants from both MPS and non-MPS sputum and tracheal aspirates were prepared and standardized to contain an identical cystatin C amount (2.9 μg). Recombinant cathepsin L was activated in the assay buffer: 100 mM sodium acetate, pH 5.5, 0.01 % Brij35, containing 2 mM DTT for 5 min at 37 °C prior to enzymatic assays. The residual peptidase activity of cathepsin L (0.5 nM) was monitored in the absence and presence of individual specimens in the assay buffer, using Z-Phe-Arg-AMC (5 μM) as a substrate (λ_{ex} = 350 nm, λ_{em} = 460 nm, Spectramax Gemini spectrofluorometer, Molecular Devices, Saint Grégoire, France). The same protocol was repeated with MPS samples, which were pretreated beforehand with glycosidases (heparinase I, II, and III, chondroitinase B, and Δ-4,5-glycuronidase) (180 mU/mL), sodium chromate (10 mM), and Dnase I (100 mU/mL) during 48 h at 37 °C under vigorous stirring. Measurements were performed in triplicates and repeated three times independently. Data are reported as mean ± standard deviation (S.D.).

3.6. Inhibition of cathepsin L by cystatin C in the presence of GAGs

Recombinant hCC was titrated with E-64-titrated commercial papain (Naudin et al., 2010). Cathepsin L (0.5 nM) activity was measured with hCC (3 nM) in the absence and presence of individual GAG (HS, DS, C4-S, C6-S, and Hep; 0–0.05 %, w/v) in the activity buffer using Z-Phe-Arg-AMC (5 μM) as a substrate. Trials were also repeated with HS dp2 and HS dp4 (0.01 %) (n = 3), and data were reported as mean ± S.D..

3.7. Kinetic measurement (determination of K_i)

Inhibition constant (K_i) was determined under experimental conditions such that nonlinear dose-response curves were obtained as described previously (Bieth, 1980), and fitted by using the Easson and Stedman plot (GraphPad Software, La Jolla California USA). Under these experimental conditions, cathepsin L concentration was at least 1–10 higher than the K_i value and <5 % of the substrate (Z-Phe-Arg-AMC) was hydrolyzed during the progress of the experiments. Ki values were calculated according to the following equation: $[I]/1 - a = (K_i/a) + E^0$, where I is the cystatin C concentration, E^0 the cathepsin L concentration at time 0, and a is the fractional activity, *i.e.*, the ratio between the enzyme activity in the presence (v_i) and absence (v_0) of hCC. The plot yields a straight line whose slope is Ki. Data are reported as mean ± S.D. (n = 3). A similar protocol was repeated in the presence of HS (0.05 %, w/v).

3.8. Microtiter plate binding assays

ELISA plate wells (Nunc MaxiSorp; Thermo Fisher Scientific) were coated either with GAGs (C4-S, HS, HS dp2, and HS dp4; 0.01 %, w/v) in the presence of BSA (100 ng/well) or with the same amount of mocked-treated BSA, and incubated overnight at room temperature, according to a protocol adapted from (Najjam et al., 1997). After three washing with PBS, containing 0.1 % (v/v) Tween 20 (PBS-T), free binding sites were blocked by a saturation buffer (PBS-T, containing BSA (100 μg/mL)) for 3 h at room temperature. Plates were washed again (three times with PBS-T, and once with distilled water) and then dried. Increased amounts of hCC (0–70 μM) dissolved in PBS containing BSA (100 μg/mL) were added in each well for 3 h at room temperature. Subsequently, plates were washed, before addition of mouse anti-cystatin C (1:1000 in PBS containing BSA (100 μg/mL)) in each well and incubation overnight at 4 °C under gentle agitation. After 3 washes with PBS-T, wells were incubated with peroxidase-conjugated mouse anti-goat IgG (1:2000 for 1 h in PBS containing BSA (100 μg/mL)) for 3 h at room temperature. After washing, a streptavidin-HRP conjugate (100 ng/mL) with BSA (100 μg/mL), then TMB (3,3′,5,5′-tetramethylbenzidine) were sequentially added. Enzyme reaction was stopped by 3 M H_2SO_4, and the absorbance was measured at 450 nm (Microplate Reader VersaMax, Molecular Devices, St Grégoire, France). The specific absorbance was deduced from the difference between the absorbance obtained from GAG/BSA-coated wells, and GAG free-BSA-coated wells, which were used as control (background noise). Equilibrium binding constants (K_D) were then calculated by linearization of the curves as described elsewhere (Orosz & Ovádi, 2002).

3.9. Circular dichroism (CD) spectroscopy

CD spectra of cystatin C (10 μM) were determined using a Jasco J-810 spectropolarimeter (Jasco France, Bouguenais, France) equipped with a Peltier thermostat system. The path length of the cell was 0.1 cm (Hellma, VWR International SAS, Fontenay-sous-Bois, France). Far UV measurements (190–240 nm) were performed at 37 °C. CD spectra of hCC were recorded in 0.1 M sodium phosphate buffer, pH 5.5 after 15 min of incubation in the absence and presence of C4-S, HS, HS dp2, and HS dp4 (0.05 %). A CD control assay was done with each GAG. Data acquisitions were made at 1 nm intervals with a dwell time of 1 s between 190 and 240 nm and averaged from three repeated scans. The secondary structure content of hCC was assessed by deconvolution of the CD spectra using free online software (Beta Structure Selection, https://bestsel.elte.hu/foldrecog.php).

3.10. Molecular docking procedure

Autodock 3 (Morris et al., 1998) was used for docking experiments using crystal human cystatin C structure (PDB ID: 3GAX, 1.70 Å) (Kolodziejczyk et al., 2010) as a receptor. Six GAG oligosaccharide ligands used for docking were as follows: heparin (IdoA(2*S*)-GlcNS(6*S*), Hep), desulfated heparin (GlcA-GlcNAc, de-Hep) and four major sulfated heparan sulfate (HS1-4) structures, which are representative HS sequences, made up of the following repetitive disaccharide units: 1) GlcA-GlcNS (HS1); 2) IdoA(2*S*)-GlcNS (HS2); 3) GlcA-GlcNS(6*S*) (HS3); 4) IdoA(2*S*)-GlcNAc(6*S*) (HS4). Another purpose of using several different HS sequences together with de-Hep and Hep was to find out if the interactions are purely electrostatics-driven, and therefore are stronger with the higher sulfation degree or are partially specific. The

ligands were built from sulfated GAG monomeric unit libraries with degree of polymerization 2 and 4 (dp2 and dp4) (Pichert et al., 2012; Samsonov et al., 2015). A grid box containing the whole human cystatin C molecule with dimensions of 126 Å × 126 Å × 126 Å and with the default grid step of 0.375 Å was applied. 100 runs of the Lamarckian genetic algorithm with an initial population size of 300 and a termination condition of 10^5 generations and 9995 × 10^5 energy evaluations were carried out. Next, 50 top energetically favorable docking results were clustered with the DBSCAN algorithm (Ester et al., 1996).

3.11. Molecular dynamics simulations

A selection of five representative structures from each cluster was chosen for molecular dynamics (MD) simulations with AMBER16 (Case et al., 2017) program using ff14SBonlysc (Nguyen et al., 2014) and GLYCAM06-j (Kirschner et al., 2008) force field parameters for protein and GAGs, respectively. The MD simulations were performed in periodic boundary conditions with TIP3P (Kirschner et al., 2008) octahedral water box with 10 Å distance from any complex atom in each direction to the box boundary. All initial structures were neutralized by counter ions (Na^+, Cl^-). The MD equilibration protocol was divided into 4 steps as described before (Maszota-Zieleniak et al., 2021). Two steps of the energy minimization were performed to remove close contacts between atoms. In the next step, the system was heated up to 300 K for 10 ps, then simulations were carried using constant temperature and pressure (NTP ensemble) until the density has been stabilized at around 1 g/mL. After the system equilibration, 25 ns MD production simulation was carried out at constant pressure using NTP ensemble (with 2 fs time step, the cut-off for non-bonded interactions 8 Å, the Particle Mesh Ewald procedure and SHAKE algorithm). Analysis of trajectories was done using the AMBER Tools 17 (Wang et al., 2006) and visualized by VMD (Humphrey et al., 1996) and Pymol (The PyMOL Molecular Graphics System, version 2.0 Schrödinger, LLC).

4. MM-GBSA binding free energy analysis and per residue decomposition

The AMBER16 program using Molecular Mechanics Generalized Born Surface Area (MM-GBSA) with igb = 2 (Onufriev et al., 2002) was used for the energetic post-processing of the trajectories and for per residue decomposition. The MM-GBSA analysis was done for all frames of the MD production run. Obtained values for the binding free energy are made up of explicit enthalpy and implicit solvent entropy, and therefore should be understood so rather as strict values of free energy of binding. Statistical analysis and graphical presentation of the obtained data were performed by R-package (http://www.R-project.org). Computational data were expressed as mean ± S.D. unless otherwise stated.

4.1. Statistical analysis

Data were expressed as median ± interquartile or mean ± S.D. Statistical significance between the different values was analyzed by non-parametric Mann-Whitney *U* test or Kruskal Wallis test, using GraphPad Prism (GraphPad software, San Diego, CA, USA). Differences at a *P*-value < 0.05 were considered significant.

5. Results

5.1. Expression level of cystatin C in MPS-I, -II, and -III patients

Lung tissue sections of a post-mortem 2-year-old female with MPS-I were stained for the presence of cystatin C. Pathological findings of the lung biopsy were reported elsewhere (Gupta et al., 2013). Of note, we earlier reported a marked accumulation of GAGs in all lung tissue sections and particularly in macrophages (Chazeirat et al., 2021). Immunoreactive hCC was predominantly localized in bronchial cells and alveolar macrophages (Fig. 1), suggesting that macrophages and bronchial cells are a source of cystatin C in lungs.

This was supported by performing ELISA studies in respiratory specimens (*i.e.*, cell-free supernatants from induced sputa and tracheal aspirates) of MPS-I, -II, and -III patients and non-MPS patients. Indeed, quantitative assessment revealed a significantly 7-fold higher level of cystatin C (median value = 181.1 ng/mL) in MPS patients *vs* non-MPS control group ($P < 0.05$) (Fig. 2A). Nevertheless, there were no confident differences of concentration between MPS-I, -II, and -III patients (Fig. 2B), suggesting that increased levels of hCC are not statistically correlated with the type of the MPS (for detailed characteristics, see (Chazeirat et al., 2021)). Our result was substantiated by immunoblotting respiratory specimens of both MPS and non-MPS patients with an anti-cystatin C antibody (Fig. 2C). Bands of higher molecular mass, which could correspond to dimeric and tetrameric forms of hCC, were detected in one MPS-III patient (Jurczak et al., 2016). The presence of such hCC oligomers, which essentially relate to pathophysiological conditions need to be confirmed and will require further investigation.

Due to the unsuitability to monitor respiratory function in young MPS patients (Denamur et al., 2022), we previously developed an alternative method, termed global respiratory symptoms severity (GRSS) to provide information on potential lung function restriction (Chazeirat et al., 2021). Briefly, GRSS is a score graduated from 0 to 4, which relies on four clinical evaluations, including ear-nose-throat symptoms, pulmonary symptoms, clinical symptoms of obstructive sleep apnea, and skeletal abnormalities causing restrictive lung disease. Interestingly, the GRSS score assigned for each patient (MPS and non-MPS) correlated positively ($rs = 0.71$, $P < 0.001$) with hCC concentration. Albeit GRSS score correlated positively with HS concentration ($r_s = 0.91$, $P < 0.0001$) as previously reported (Chazeirat et al., 2021), we did not observe a significant correlation between hCC and HS or DS levels, the two accumulated GAGs in MPS-I, -II and -III patients, despite a slightly definite trend with total sulfated GAGs levels ($rs = 0.59$, $P < 0.0057$).

These findings suggest that there is no apparent link on both the nature and the concentration of GAGs, and the increased amount of hCC in respiratory specimens of MPS patients. Besides serum creatinine, which is a routine biomarker for evaluation of glomerular filtration rate, it is well established that serum hCC is also a valuable earlier marker of acute kidney injury (Grubb, 2010; Schiffl & Lang, 2012). Here, no significant differences of renal clearance and serum creatinine levels were observed in non-MPS *vs* MPS patients, supporting that the significantly higher level of cystatin C found in respiratory specimens of MPS patients *vs* non-MPS control group may be specifically associated to GRSS score (Table 1).

Data are presented as mean ± standard deviation (S.D.). No significant differences in age, size, weight, serum creatine levels, and clearance were observed. The other clinical characteristics from MPS and non-MPS patients were reported elsewhere (Chazeirat et al., 2021).

5.2. Glycosaminoglycans in sputa and tracheal aspirates from MPS patients impair the inhibitory potential of cystatin C

Although inhibitory properties of several inhibitors of serine proteases and metallo-proteases, are known to be modulated by GAGs (Rein et al., 2011; Tocchi & Parks, 2013), most notably heparin (Hep) and HS, the ability of GAGs to regulate hCC, the most potent inhibitor of cysteine cathepsins (Abrahamson et al., 2003; Turk et al., 2008), has not yet been investigated. First, we initially examined the inhibitory potential of hCC in MPS patients. For the sake of unambiguous analysis of data, we selected as an enzyme model human cathepsin L, which does not bind to GAGs and which catalytic activity and stability are unaffected by GAGs, contrary to other related cathepsins K, S, and V (Bojarski et al., 2022; Li et al., 2000). Four serial dilutions of cell-free supernatants of MPS respiratory specimens (1:20, 1:200, 1:2000, and 1:20000, corresponding to

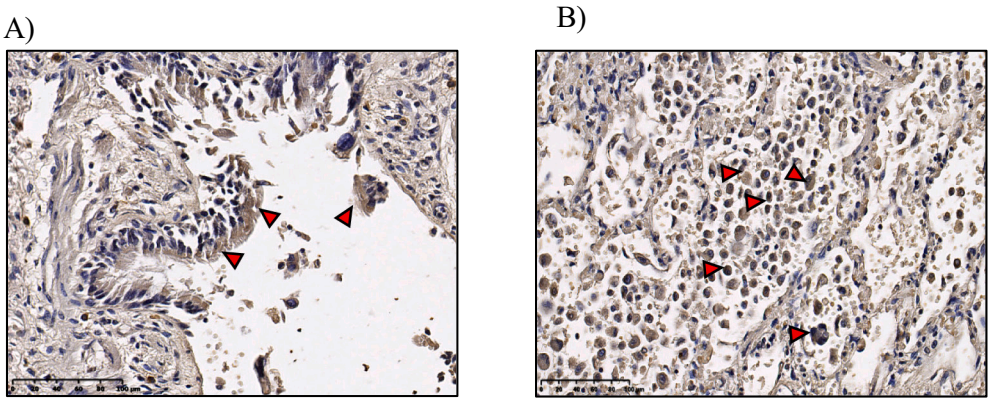

Fig. 1. Immunohistochemistry of cystatin C in human lung MPS-I tissue.
Cystatin C staining was performed on lung tissue obtained from a post-mortem 2-year-old female with MPS-I. Cystatin C (dark brown staining) was detected in bronchial cells (panel A, ×300) and in alveolar macrophages (panel B, ×300), as indicated by red arrowheads (scale bar: 100 μm). (For interpretation of the references to colour in this figure legend, the reader is referred to the web version of this article.)

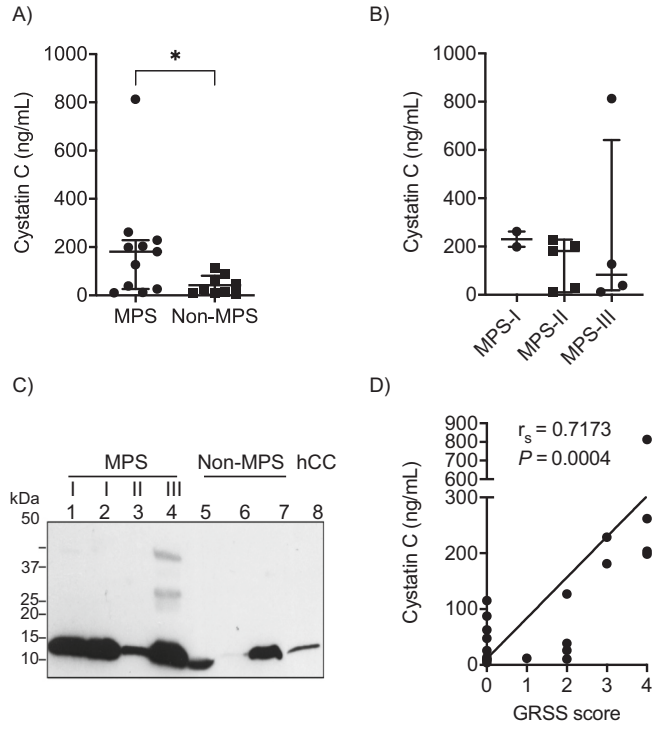

Fig. 2. Cystatin C levels in respiratory secretions from non-MPS and MPS-I, II, and III patients.
A) ELISA protein levels of hCC in cell-free supernatants of induced sputum and tracheal aspirates of individual non-MPS (N = 9) and MPS patients (N = 11), which included MPS I (N = 2), MPS II (N = 5), and MPS III (N = 4). B) Levels of hCC in MPS I (N = 2), MPS II (N = 5), and MPS III (N = 4). C) Representative western-blot (of two independent experiments) of hCC expression from three MPS patients (I, II, III) (lanes 1–4) (lanes 1 and 2 correspond to tracheal aspiration and sputum, respectively, both from a patient MPS-I) and three non-MPS patients (lanes 5–7). The other MPS and non-MPS samples were not shown due to their limited availability for western blot. A fixed amount of each sample (375 μg of total protein/well) was deposited on SDS-PAGE (4–20 %), under reducing conditions. Recombinant human cystatin C (Cyst C, 20 ng) was deposited as a control (lane 8). D) Individual data of cystatin C levels related to respiratory symptoms in MPS patients are presented with the following rating: 1: low; 2: moderate; 3: important; 4: severe. The plot was completed by linear regression. Spearman coefficient (rs) and level of significance (*P*) were reported. Statistical analyses were performed using Mann-Whitney *U* test (*: $P < 0.05$). Results are expressed as median ± interquartile range of three independent experiments.

300, 30, 3 ng, and 0.3 ng of total protein, respectively) from MPS patients were incubated in the activity buffer (pH 5.5) with a constant amount of recombinant cathepsin L (0.5 nM), before measuring the residual activity by Z-Phe-Arg-AMC (Fig. 3A). Interestingly, no decrease in cathepsin L activity was observed in any MPS types, regardless of sample dilution and MPS grade. Of note, no endogenous peptidase activity was detected in the diluted MPS samples, prior addition of ectopic cathepsin L. Taken together this quite unexpected maintenance of peptidase activity and both elevated levels of hCC and sulfated GAGs (Fig. 3B) in MPS samples led us to investigate whether GAGs may modulate the inhibitory potential of hCC toward cathepsin L. To answer this intriguing question, we diluted the different respiratory specimens to have a constant normalized amount of endogenous cystatin C (2.9 μg), then measured the residual activity of ectopic cathepsin L. Again, no decrease in cathepsin L activity was observed in MPS samples. In contrast, pretreatment of these samples with glycosidases (heparinases I, II, and III, chondroitinase B and Δ-4,5-glycuronidase) yielded a potent and significant inhibition of cathepsin L ($P < 0.0001$) (Fig. 3C). An identical result was retrieved with non-MPS specimens in the absence of treatment with glycosidases ($P < 0.0001$). Data show that the ability of hCC to inhibit ectopic cathepsin L depends on the removal of GAGs.

Table 1
Clinical characteristics from non-MPS and MPS patients.

Patients	Age (year)	Height (cm)	Weight (kg)	Creatinine (μmol/mL)	Clearance (mL/min)
Non-MPS (N = 9)	9 ± 6	133.0 ± 41	34.0 ± 22	36 ± 11	110 ± 24
MPS (N = 11)	10 ± 6	112.3 ± 18	26.5 ± 11	30 ± 9	148 ± 42

5.3. Heparan sulfate and heparin modulate the inhibitory activity of cystatin C

Recombinant hCC was used to analyze the specific regulation of hCC inhibitory potency by GAGs. We chose experimental conditions such ~80 % of cathepsin L activity was inhibited by hCC in the absence of GAGs. Then, incubation was conducted in the presence of 0.05 % (w/v) C4-S, C6-S, Hep, DS, and HS, before monitoring the residual peptidase activity of cathepsin L. It is noteworthy that the chosen GAG concentration range, *i.e.*, 0.05 % (w/v), corresponds to that determined in clinical samples from MPS patients (Chazeirat et al., 2021; Chung et al., 2007; Haskins et al., 1992). Hep and HS, but not DS, C4-S and C6-S, significantly impaired cathepsin L inhibition by cystatin C ($P < 0.01$) (Fig. 4A).

Moreover, a HS dose-dependent lack of inhibition was observed and cathepsin L activity was restored in the presence of 0.05 % (w/v) HS ($P < 0.01$) (Fig. 4B). Of note, either preincubation of cathepsin L with hCC prior adding HS or preincubation of hCC with HS prior adding cathepsin

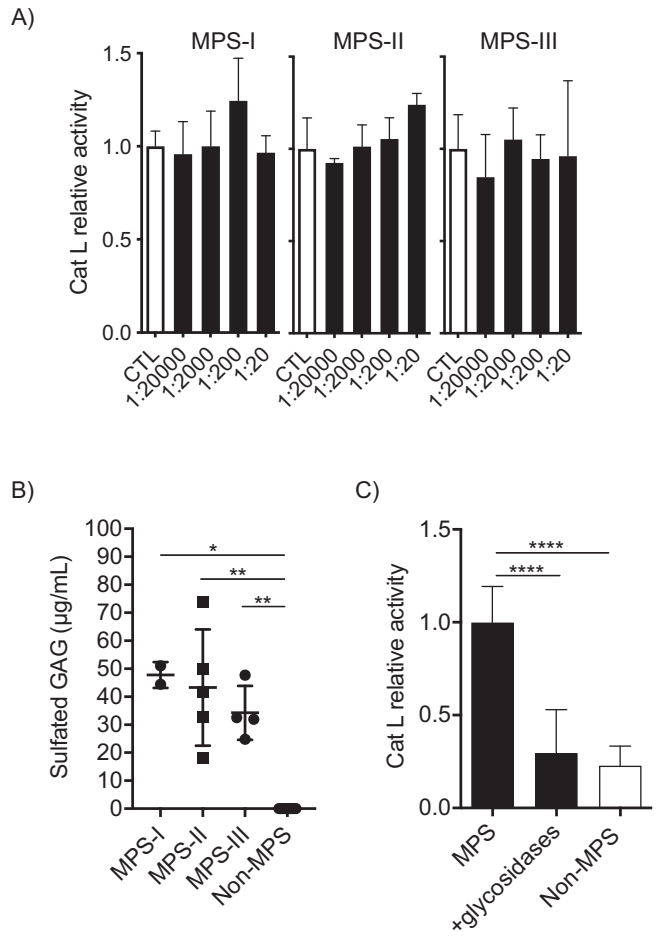

Fig. 3. Comparison of hCC inhibitory potential toward cathepsin L in MPS and non-MPS patients.
A) Recombinant human cathepsin L (Cat L, 0.5 nM) was incubated for 10 min in the activity buffer alone (control: CTL) or with different dilutions of cell- free supernatants from individual respiratory secretion of MPS-I (N = 2), MPS-II (N = 5), MPS-III (N = 4). Residual activity (triplicate) was measured with Z-Phe-Arg-AMC (5 µM) and compared to control (activity = 1). B) Sulfated GAG levels in MPS-I, -II, and -III (N = 11) and non-MPS (N = 9) patients. C) Comparison of Cat L activity in respiratory secretions from non-MPS and MPS-I, -II, and -III patients. Cat L (0.5 nM) was incubated for 10 min in the activity buffer with each cell-free supernatants from respiratory secretions of non-MPS (N = 9) and MPS (N = 11). Starting biological samples were all equivalent in hCC content (2.9 µg). The same experiment was carried out with each MPS sample pre-treated with glycosidases (heparinases I, II, III, and Δ-4, 5-glycuronidase). Residual activity (triplicate) was measured with Z-Phe-Arg-AMC (5 µM) and compared to MPS (activity =1). Statistical analyses were performed using Mann-Whitney *U* test (*: $P < 0.05$; **: $P < 0.01$; ***: $P < 0.001$; ****: $P < 0.0001$). Results are expressed as mean ± S.D. of three independent experiments.

L gave similar results. Inhibition constant (K_i) in the presence and absence of 0.05 % (w/v) HS were further determined as described in the experimental section. Although hCC displayed a potent inhibitory potential for cathepsin L under both conditions, hCC was 10-fold less potent ($K_i = 1.5 \pm 0.3$ nM) in the presence of HS (0.05 %) than in the absence of HS ($K_i = 0.16 \pm 0.9$ nM), suggesting that HS may lower the regulatory role of hCC in MPS patients.

Next, we aimed to evaluate whether electrostatic interactions could critically govern binding of negatively charged HS to positively charged cystatin C (pI: 9.3) (Popović et al., 1990). Nevertheless, under present experimental conditions, cathepsin L activity was weakened in a concentration-dependent manner by increasing ionic strength (*i.e., circa* 70 % remaining peptidase activity in the presence of 300 mM NaCl), thus preventing us to evaluate whether the presence of NaCl can dissociate HS-hCC complex.

5.4. Structural oligosaccharide motifs of HS involved in cystatin C binding

Alternatively, we used HS oligosaccharides with defined lengths to identify critical structural elements required for binding of HS to hCC. Accordingly, we analyzed the ability of two HS-derived disaccharides and tetrasaccharides, dp2 and dp4 (dp: degree of polymerization), to modulate the activity of hCC toward cathepsin L (Fig. 4D). The observed recovery of cathepsin L activity was approximately 2-fold greater ($P < 0.0001$) in the presence of HS dp2 (0.01 %) than that measured for hCC alone. This result indicates that a disaccharide is the minimal length required to modulate the inhibitory capacity of hCC. Furthermore, as the structure of heparinase III generated disaccharides is Δ(4,5)hexuronic acid (1–4)GlcNAc ± 6S, this suggests that the nature of the uronic acid may not be critical for hCC recognition. Moreover, we observed a significant ~3-fold increase of cathepsin L activity recovery with oligosaccharide HS dp4 (0.01 %), suggesting that HS oligosaccharides binds to hCC in a chain-length dependent fashion ($P < 0.001$). Equilibrium binding constants (K_D) between cystatin C and immobilized C4-S, HS, HS dp2, and HS dp4 were further determined by microtiter plate binding assays (Fig. 5A). Cystatin C bound to C4-S, HS, HS dp2, and HS dp4, with substantially different K_D. C4-S bound to hCC with weaker affinity ($K_D >$ 19 µM) than HS ($K_D = 5.5 \pm 2.3$ µM), in agreement with former results. In contrast, hCC bound to HS dp4 ($K_D = 0.05 \pm 0.03$ µM) with a higher affinity than HS dp2 ($K_D = 0.66 \pm 0.2$ µM) and HS, supporting previous finding (Fig. 4D).

Next, for structural analysis, the near-UV CD spectra for hCC in the absence and presence of C4-S, HS, HS dp2, and HS dp4 (0.05 %) were measured (Fig. 5B). The percentage of secondary structure motifs of hCC, which was calculated by Bestsel algorithm, were 7.2 % α-helix, 35.6 % β-sheets, 14.1 % β-turns, and 43.1 % random coil, in agreement with those reported in literature (Calero et al., 2001). In the presence of C4-S, the CD spectra of hCC showed relatively similar curves, indicating that C4-S displayed minor effect on the overall protein folding. In contrast, a noteworthy increase in α-helix content (18.6 %) was observed in the presence of HS, compared to hCC alone (7.2 %), while β-turn content was comprehensively reduced. These data support that binding of full-length HS to hCC led to a deep reorganization of its secondary structure and, subsequently, of its tertiary structure. In contrast, binding of both HS dp2 and dp4 oligosaccharides resulted in more restrained structural changes, reflected by a higher β-sheet content while the predicted α-helix content of hCC (HS dp2: 6.9 %, and HS dp4: 7.8 %) remained similar to unbound hCC.

5.5. Molecular modeling of GAG oligosaccharides (dp2 and dp4) binding to cystatin C

The structure of monomeric hCC in solution is characterized by five-stranded antiparallel β-sheets wrapped around a long a-helix, which lies orthogonally onto the β-strands, two hairpin loops (L1 and L2), and the so-called appending structure (AS) (Perlenfein et al., 2017). The three regions of cystatin C involved in the interactions with target proteolytic cysteine proteases are highly conserved among cystatins and located one in the flexible N-terminal fragment and two in β-hairpin loops that connect strands 2 and 3 (L1), and 4 and 5 (L2) (Fig. 6A). The N-terminal proteinase interacting wedge comprised residues Arg8-Gly11 and the two loop fragments L1 and L2 involved residues Gln55-Gly59, and Pro105-Trp106, respectively. To gain a better understanding of the experimental results with HS at the atomistic level, molecular docking (MD) followed by MD simulations were performed. HS consists of alternating *N*-acetylglucosamine (GlcNAc) and hexuronic acids (glucuronic acid, GlcA or its C-5 epimer iduronic acid, IdoA) disaccharide repeating units. Various predominant types of sulfation modifications

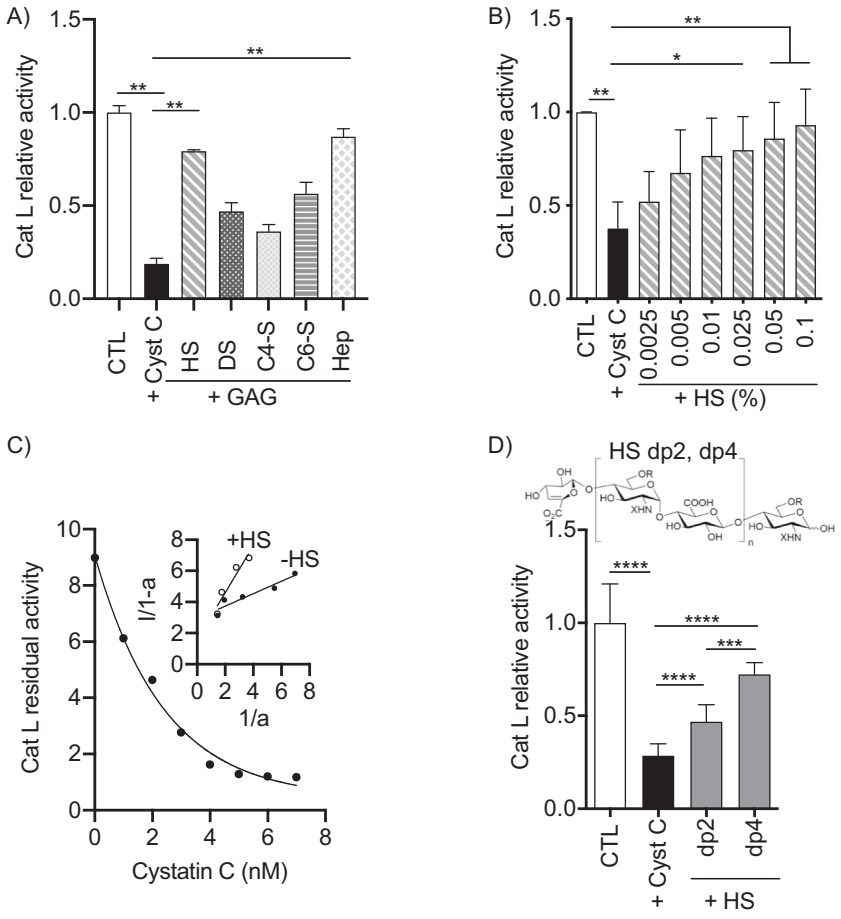

Fig. 4. Alteration of hCC inhibitory potential in the presence of HS.
A) Cat L (0.5 nM) was incubated in the absence (control, CTL) and presence of recombinant hCC (3 nM) and different GAG (HS: heparan sulfate; DS: dermatan sulfate; C4-S/C6-S: chondroitin 4/6-sulfate; Hep: low molecular weight heparin) at 0.05 % (weight/volume, w/v) in the activity buffer. B) Cat L (0.5 nM) was incubated alone, with hCC (3 nM) in the absence and presence of increasing concentrations of HS (0–0.1 %). C) Determination of the inhibition constant (K_i) of Cat L and hCC in the absence and presence of HS (0.05 %). The residual enzymatic activity of Cat L was measured by incubating the enzyme with increasing concentrations of hCC (black symbol). An Easson-Stedman plot (inset) was used to calculate the K_i (hCC; hCC + HS). A representative curve of three experiments is shown. D) Cat L (0.5 nM) was incubated alone, with hCC (3 nM) in the absence and presence of HS dp2 and HS dp4 (0.01 %). Structure of HS dp is represented above: Δ(4,5)hexuronic acid (1-[4)GlcNAc/S ± 6S (1–4)GlcA(1]n-4)GlcNAc ± 6S, where n = 0 (dp2) and 1 (dp4), R = SO_3^- or H and X = SO_3^- or $COCH_3^-$. Statistical analyses were performed using Mann-Whitney *U* test (*: $P < 0.05$; **: $P < 0.01$; ***: $P < 0.001$; ****: $P < 0.0001$). Results are expressed as mean ± S.D. of three independent experiments.

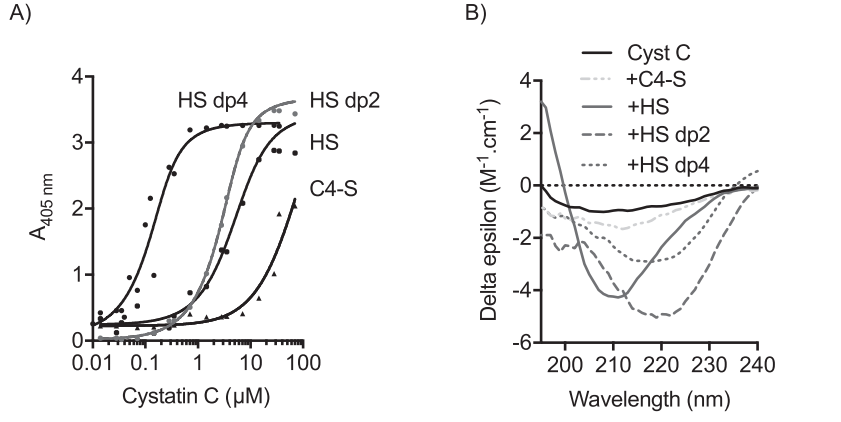

GAG	K_D (μM)
HS	5.5±2.3
C4-S	>19
HS dp2	0.66±0.2
HS dp4	0.05±0.03

	α-helix (%)	β-sheet (%)	β-turn (%)	others (%)
Cyst C	7.2	35.6	14.1	43.1
+C4-S	4.3	35.0	12.9	47.8
+HS	18.6	32.5	8.7	40.1
+HS dp2	6.9	45.0	12.8	35.3
+HS dp4	7.8	43.2	17.2	31.7

Fig. 5. Interaction between hCC and C4-S, HS, and HS oligosaccharides.
A) Binding of hCC with GAG by microtiter plate binding assays. Plates were coated with individual GAG (C4-S, HS, HS dp2, and HS dp4) and probed with increasing concentrations (10 nM–70 μM) of hCC. K_D values were determined (mean ± S.D., n = 3). B) Circular dichroism spectra of hCC with C4-S, HS, and HS derivatives. Cystatin C (10 μM) was incubated alone or with 0.05 % of C4-S, HS, and HS oligosaccharides (dp2 and dp4). Corresponding Far UV CD spectra (195–240 nm) of hCC (Cyst C) were recorded in 0.1 M sodium phosphate buffer, pH 5.5 (37 °C). Baseline recordings were performed before each assay and subtracted to each GAG spectrum. Data (expressed as mean residue ellipticity) were averaged from three repeated scans. The experimental secondary structure content of cystatin C was calculated by deconvolution of the CD spectra (Beta Structure Selection, https://bestsel.elte.hu/foldrecog.php).

are present in HS, including *N*-, 2-*O*-, and 6-*O*-sulfates (NS, 2S, and 6S, respectively) (Annaval et al., 2020). Thereby, we analyzed several major HS oligosaccharides (dp2 and dp4) combinations as well as Hep, and de-sulfated Hep (de-Hep). Among the fifty top-ranked complexes obtained, major differences in the docking poses between dp2 and dp4 were observed (Fig. 6B). Among dp2 oligosaccharides, only Hep dp2 bound to the N-terminal region of hCC, while all dp4 oligosaccharides were docked in the N-terminal fragment. The docking poses for HS2 and HS3

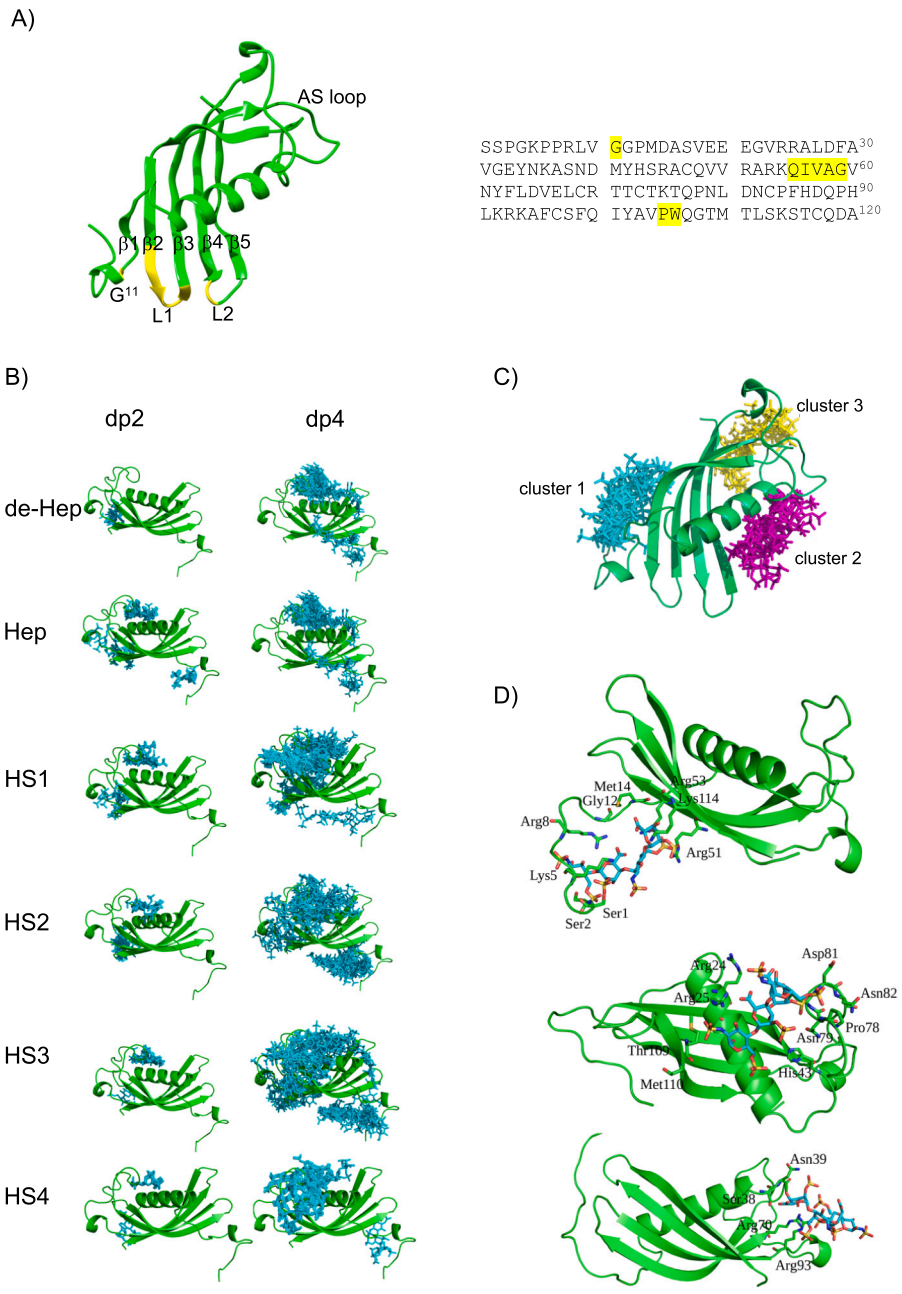

Fig. 6. *In silico* interactions between hCC and GAG oligosaccharides.
A) hCC sequence (Uniprot ID: P01034). Residues involved in enzyme binding region are underlined in yellow. B) Top 50 docking poses obtained for hCC (green) and GAGs dp2 and dp4 (cyan). C) The three major clusters of Hep dp4 (cyan, magenta, yellow) structures docked to hCC. D) The major amino acids of hCC (green) involved in the binding to Hep dp4 (cyan) identified by MD simulations (carbon: green, nitrogen: blue, oxygen: red), which correspond to, from the top to the bottom: hCC/Hep dp4 (pose 1), hCC/Hep dp4 (pose 2), and hCC/Hep dp4 (pose 3). (For interpretation of the references to colour in this figure legend, the reader is referred to the web version of this article.)

dp4 are the most representative in this region. Most of the obtained docking poses, for both dp2 and dp4 ligands, are found in the AS loop region. The exception is de-Hep dp2, where all top 50 poses are located near the fragment connecting α-helix with first β-sheet.

The best scored solutions were then clustered, and five representative poses of each cluster were taken for MD simulations. Most of the cystatin C-GAG complexes were stable during the simulation, the less stable ones were hCC-HS4 dp4 complexes, for which several dissociation events were observed (Supplementary Fig. 1). Furthermore, the MM-GBSA binding free energy (ΔG) analysis was performed for hCC-GAG complexes and the correspondence of the binding sites and specific clusters to binding energies are summarized in Table 2. The most stable and recurrent interactions were obtained with the N-terminal fragment and Hep dp4 (−36.4 kcal/mol), HS2 dp4 (−34.2 kcal/mol), and HS3 dp4 (−36.1 kcal/mol). Another stable interaction was detected between the hCC fragment (located between L2 and AS loop) and HS1 dp2 (−32.6 kcal/mol). The increase of the GAG length of Hep, de-Hep, and HS2 favored complex formation, while it induced weaker interactions for HS4. Finally, three representative structural clusters of docking poses were found in hCC, which are closely to the N-terminal fragment (cluster 1), the AS fragment (cluster 2), and the fragment between α-helix with first β-sheet (cluster 3) (Fig. 6C). Additional binding sites were predicted near the last β-sheet of hCC and between the L2 and AS loops. Although the AS loop is the most populated binding site for GAGs, it does not correspond to the most energetically favorable pose, which were obtained for the oligosaccharides docked at the N-terminus of hCC. Furthermore, and supporting the importance of this specific GAG binding region, in several MD simulations, the oligosaccharide dissociation from the primary binding site was followed by the interactions with the N-terminus. Although the modeled interactions are in general stronger upon the increase of the net sulfation per GAG disaccharide unit, there are also indications that these interactions are partially specific and not exclusively determined by the net charge, as illustrated by the difference in ΔG values between HS2, HS3, and HS4, which have

Table 2
MM-GBSA binding free energy (ΔG) analysis of cystatin C-GAG complexes.

GAG	Cluster number	ΔG[a] (kcal/mol)	ΔG[a] per cluster (kcal/mol)	Location
Hep dp 2	1	−18.6 ± 11.0	−18.0 ± 10.1	AS loop
	2		−27.1 ± 10.6	N-ter segment
	3		−10.6 ± 6.2	Segment connecting α-helix with first β-sheet
Hep dp 4	1	−29.1 ± 11.1	−36.4 ± 7.0	N-ter segment
	2		−25.5 ± 12.5	AS loop
	3		−24.5 ± 11.5	Segment connecting α-helix with first β-sheet
de-Hep dp 2	1	−13.4 ± 7.9	−13.4 ± 7.9	Segment connecting α-helix with first β-sheet
de-Hep dp 4	1	−14.0 ± 8.8	−11.3 ± 6.1	AS loop
	2		−16.7 ± 10.8	Between L2 and AS loop
HS1 dp2	1	−17.3 ± 12.3	−32.6 ± 4.9	Between L2 and AS loop
	2		−8.0 ± 5.8	AS loop
	3		−11.3 ± 5.7	AS loop
HS1 dp4	1	−16.0 ± 8.8	−14.1 ± 8.3	AS loop
	2		−17.8 ± 9.7	Close to the last β-sheet
HS2 dp2	1	−13.4 ± 9.0	−15.5 ± 10.4	AS loop
	2		−11.3 ± 7.9	Segment connecting α-helix with first β-sheet
HS2 dp4	1	−20.3 ± 12.5	−14.5 ± 9.4	Between L2 and AS loop
	2		−10.2 ± 4.0	N-ter segment
	3		−34.2 ± 4.4	N-ter segment
HS3 dp2	1	−35.1 ± 6.2	−35.1 ± 6.2	AS loop
HS3 dp4	1	−28.2 ± 11.6	−36.1 ± 10.5	N-ter segment
	2		−20.5 ± 8.7	segment connecting α-helix with first β-sheet
HS4 dp2	1	−20.9 ± 4.4	−20.9 ± 4.4	AS loop
HS4 dp4	1	−8.0 ± 5.6	−13.1 ± 4.1	AS loop
	2		−7.6 ± 1.2	AS loop
	3		−5.1 ± 5.6	AS loop

[a] ΔG values are expressed as mean ± S.D.

the same net charge. The net charge of de-Hep, HS1, HS2, HS3, HS4, and Hep disaccharide units is −1, −2, −3, −3, −3, −4, respectively.

To analyze in more detail hCC-GAG binding sites, MM-GBSA free binding energy per residue decomposition was performed. The ten energetically most favorably contributing residues from each cluster were compared for different GAGs (Supplementary Table 1). We selected only residues that were present at least twice in a cluster and had a ΔG value below −1 kcal/mol. Cystatin C-Hep dp4 complex was chosen to illustrate our observations since all three binding poses were representative for all GAGs, and moreover, the binding free energy was the lowest for all tested hCC-GAG complexes, for which all three clusters were obtained. Key residues that are involved in the stabilization of the complexes localize in three main regions, including primarily N-ter residues (cluster 1), residues of the α-helix, AS loop and the last β-sheet (cluster 2), and a region that is stabilized by interactions between the GAG and Ser38, Asn39, Arg70, and Arg93 (cluster 3) (Fig. 6D).

6. Discussion

We previously investigated the influence of HS, the most prominent type of GAG accumulated in MPS type I, II, and III to bind and inactivate in a dose dependent manner human cathepsin V, the most potent elastolytic mammalian protease reported yet, and which is implicated in the extracellular matrix remodeling (Chazeirat et al., 2021). Also, we reported that HS level in respiratory specimens from MPS-I, -II, and -III patients correlated positively with the severity of respiratory symptoms (GSSR), albeit the overall endopeptidase activity of cysteine cathepsin proteases was negatively related to GSSR. Here, we turned our attention to hCC, a circulating tight binding inhibitor of cysteine cathepsins, and its interactions with HS. We showed that hCC is expressed in alveolar macrophages and bronchial cells in lung section of MPS-I patient and its expression is upregulated in respiratory specimens of MPS-I, -II, and -III compared to controls. A growing body of evidence endorses that GAGs modulate diverse biological processes such as enzymatic activities, extracellular matrix assembly, as well cell signaling, through the regulation of growth factors, chemokines, and adhesion molecules (Vallet et al., 2022). Nevertheless, the primary mechanism to cause hCC overexpression in MPS patients is unknown. A plausible explanation is that HS-proteoglycans (HSPGs) and HS have been reported to interact with several growth factors (FGFs, VEGF, and TGF-beta) to promote their biological activities (for review: Rider & Mulloy, 2017; Shi et al., 2021). Moreover, taken together that TGF-beta activity is increased in MPS-I patients (Yano et al., 2013), and TGF-beta participates in the increase of cystatin C secretion in different cell types (Kasabova, Joulin-Giet, Lecaille, Gilmore, et al., 2014; Solem et al., 1990), suggest that HS may stimulate the expression of TGF-beta, which in turn could drive overexpression of secreted hCC. Interestingly, hCC levels correlated positively with GSSR, suggesting that an increase in hCC level can be associated with the onset of respiratory-related disorders, irrespective of the age of patients. Moreover, an upregulation of hCC serum concentration was reported in some fibrotic diseases, including multiple sclerosis (Bollengier, 1987), chronic hepatitis fibrosis (Takeuchi et al., 2001), liver fibrosis (Chu et al., 2004), oral mucosa fibrosis (Chung-Hung et al., 2007), and idiopathic pulmonary fibrosis (Kasabova, Joulin-Giet, Lecaille, Saidi, et al., 2014). On the other hand, serum hCC was proposed to be a valuable and more accurate marker of glomerular filtration rate than the widely used serum creatinine and may represent an alternative for the early assessment of acute kidney injury (for review: (Kar et al., 2018)). Accordingly, present data sustain that the increased hCC expression in MPS respiratory specimens did not rely on an impaired glomerular filtration rate associated to kidney injury, as we observed previously for IPF patients (Kasabova, Joulin-Giet, Lecaille, Saidi, et al., 2014). Under these circumstances, dosage of hCC in sputum of MPS patients may represent a reliable non-invasive biomarker in the management of severe respiratory disorders diagnosis.

Alternatively, cystatin C is a highly potent inhibitor of cysteine cathepsins, which obeys a 1:1 stoichiometric mechanism, and it is likely that its inhibitory activity increased in MPS patients. Furthermore, several reports demonstrated that specific GAGs, including Hep and HS enhance the inhibitory potency of various protease inhibitors (Higgins et al., 2010; Rein et al., 2011; Ruiz-Gómez et al., 2019). For example, GAGs accelerated inhibition of cathepsin L by squamous cell carcinoma antigens (*i.e.*, serpins B3 and B4), which are cross-class protease inhibitors (Higgins et al., 2010). Together with cathepsin B, cathepsin L is the most widely expressed lysosomal cysteine protease, playing a critical and specific role in protein processing, extracellular matrix, and tissue remodeling (Lecaille et al., 2002). Its dysregulation contributes to the initiation/progression of multiple human diseases, including lungs disorders (Bühling et al., 2004). Remarkably, we found that ectopic cathepsin L remained fully active after addition in respiratory specimens of MPS patients despite elevated HS and hCC levels. Conversely, the peptidase activity of cathepsin L was significantly reduced when samples were pre-treated with glycosidases. Hence, an excess or an accumulation of GAGs may impair hCC inhibitory activity in lung and thus potently weaken its regulatory function in MPS patients. The finding that both HS and its highly sulfated form, Hep, but not CS and DS, modulated the hCC inhibitory activity, could suggest that the degree and sulfation patterns, as well as the nature of saccharide backbone and of the glycosidic linkages may constitute structural features driving the interaction with hCC. In fact, HS and Hep consist of repetitive disaccharide unit GlcA/IdoA-GlcNAc/NS (α1–4 linkage), while CS and DS chains are constituted of the repetitive disaccharide GlcA-GalNAc and IdoA-GalNAc (β1–3 linkage), respectively. Interestingly, orthologous mouse and human cystatin C share 71 % of amino acid identity, supporting similar structural and functional properties. A recent report indicated that HS down-regulates the potency of mouse cystatin C to inhibit papain, the archetype of cysteine cathepsins, under acidic

conditions (Zhang et al., 2021), corroborating present results.

Here, presence of HS substantially compromised inhibition constant (K_i) of hCC against cathepsin L. Nevertheless, it should be noted that our experimental K_i values were at least 100-fold weaker than the one reported elsewhere (Mason et al., 1998), possibly due to a conformational change in hCC molecule within the hCC/cathepsin L complex, rendering its N-terminal substrate-like region susceptible to hydrolysis by the protease (cleavage site between Gly10-Gly11) (Popovic et al., 1999). As a result, N-terminal truncated forms of hCC, have much lower affinity for cysteine proteases than the full-length inhibitor (Abrahamson et al., 1987; Cimerman et al., 1999). Additionally, intracellular cathepsin L is critical for pro-heparanase processing into its active form that is responsible for the cleavage and release of HS side chains from proteoglycans (Abboud-Jarrous et al., 2008). Accordingly, the lack of inhibition of cathepsin L activity by hCC may sustain elevated levels of HS in MPS patients.

Next, we examined whether C4-S, Hep and HS oligosaccharides bind to hCC. Experimental data suggest that interactions between hCC and HS are sequence dependent, and we identified short HS-derived oligosaccharides that were sufficient to restore cathepsin L activity in the presence of hCC. In agreement with the lack of effect of CS or DS in the inhibitory potential of hCC, these data also indicated a requirement for a *N*-acetylated glucosamine residue, while the nature of the uronic acid was less critical. Of interest, these di- and tetrasaccharides (HS dp2 and dp4) bound more efficiently hCC than full-length porcine HS (~15 kDa). Likewise, present results corroborate a recent report claiming that mouse cystatin C bound preferentially to HS-derived hexasaccharides than longer HS oligosaccharides (Zhang et al., 2021). Also, these results are in good agreement with near-UV CD data, which support that the binding mode of HS dp2 and dp4 to hCC genuinely differs from those of the full-length HS. Accordingly, the weaker equilibrium binding constant (K_D) between hCC and HS, compared to HS dp4 and HS dp2, could reflect distinctive structural variations induced by the formation of the GAG-hCC complex, independently of the ability of HS, and both HS dp4 and HS dp2 to modulate hCC activity. On the other hand, accumulating evidence indicates that oligomerization of hCC occurs *in vivo* and is related to disease (Jurczak et al., 2016). The relative potency of HS to trigger hCC oligomerization, as observed for other proteins (*i.e.*, chemokines, (Dyer et al., 2016)) may represent an additional mechanism of regulation of hCC functions in MPS. However, the relevance of such structural rearrangements requires future investigations. Molecular modeling study predicted that the residues of hCC involved in HS dp2 and dp4 binding are allocated into three binding sites corresponding to the obtained structural clusters of docking solutions. One cluster is located at the N-terminus (cluster 1), corresponding to the residues Ser1, Ser2, Lys5, Leu9, and Gly11. Previous functional studies demonstrated that the first eleven-residues of N-terminus of hCC are of major importance for its typical tight-binding inhibition of cysteine cathepsins (Abrahamson et al., 1987). The residues preceding the evolutionarily conserved Leu9, Val10, and Gly11 target the active site of the enzyme in a substrate-like manner (Machleidt et al., 1989), supporting that HS and HS oligosaccharides may impede the binding of hCC within the substrate binding cleft of cathepsin L by interacting with the N-terminus region. In addition, the two inhibitory loop-forming hCC fragments (L1 and L2), corresponding to Gln55-Gly59 and Pro115-Trp116, respectively, were apparently not required for HS/Hep binding, suggesting that the flexible N-terminus is critical for HS binding and could explain the reduced activity of hCC toward cathepsin L. The two other clusters are located near residues of the α-helix, AS loop and the last β-sheet (cluster 2), and a region that is stabilized by interactions between the GAG and Ser38, Asn39, Arg70, and Arg93 (cluster 3). Interestingly, these results support those found for mouse cystatin C undertaken by NMR and site-directed mutagenesis studies, in which residues located at the N-terminus (Lys4 to Glu14), Arg51, and residues between Gln88 and Cys97 are important for HS binding (Zhang et al., 2021). Moreover, the binding of HS or Hep to the N-terminus resulted in an increase of helical content of mouse cystatin C, which are fully consistent with our experimental data showing that hCC led to a deep reorganization of its secondary structure (α-helix) upon HS binding.

In summary, this is the first study that evaluates the protein level of human cystatin C in respiratory specimen from MPS patients and correlates its expression with GRSS scores, which is associated to the severity of respiratory symptoms. We identified HS as an unexpected but potent modulator of the inhibitory activity of hCC. Taken together with the specific inactivation of elastolytic cathepsin V by HS (Chazeirat et al., 2021), hCC dysregulation of its inhibitory potency toward cathepsin L may in turn promote protease/antiprotease imbalance in favor to proteolysis. The structural analysis of the hCC/HS complex model presented here will facilitate further studies on the design of specific competitors aiming to prevent HS-hCC binding and ultimately restore the proteolytic cysteine cathepsin/cystatin balance. Nevertheless, future fundamental and mechanistic studies are needed to clarify *in vivo* and *in vitro* the specific role of cystatin C in lungs from MPS patients, but also in other organs such as bone and brain that are affected during MPS pathogenesis.

CRediT authorship contribution statement

FL designed research; SD, TC, MM-Z performed research; RRV, FZ, RJL, and FL contributed new reagents; TC, SD, KB, DS, SS, GL, and FL analyzed data; FL wrote the paper. SD, TC, RJL, MM-Z, SS, AS, RRV, RJL, and GL revised the paper. All authors approved the final version of the manuscript.

Declaration of competing interest

The authors declare that they have no known competing financial interests or personal relationships that could have appeared to influence the work reported in this paper.

Acknowledgments

This work received funding from the French association Vaincre les Maladies Lysosomales (VML, Massy, France) and was supported by the Institut National de la Santé et de la Recherche Médicale (INSERM), the University of Tours, the RTR MotivHealth (Région Centre-Val de Loire, France) and the CNRS GDR GAG (GDR 3739). We acknowledge the H2020 COST action CA 20113 (PROTEOCURE: a sound proteome for a sound body: targeting proteolysis for proteome remodeling). TC holds a doctoral fellowship from MESRI (Ministère de l'Enseignement Supérieur, de la Recherche et de l'Innovation, France). SD was supported by a French Pediatric Society (SFP) award. RRV is supported by the "Investissements d'avenir" program Glyco@Alps (ANR-15-IDEX-02) and by grants from the Agence Nationale de la Recherche (ANR-17-CE11-0040 and ANR-19-CE13-0031). IBS acknowledges integration into the Interdisciplinary Research Institute of Grenoble (IRIG, CEA). SS received funding (grant UMO-2018/30/E/ST4/00037) from the National Science Centre, Poland (Narodowe Centrum Nauki). Computational resources were provided by the Polish Grid Infrastructure (PL-GRID, grant plggagstr3), ZIH at TU Dresden (grant p_gag) and a local cluster at the Faculty of Chemistry, University of Gdansk. Authors acknowledge Dr. Damien Sizaret (Anatomical Pathology and Cytology department, Bretonneau Hospital, CHRU Tours, France) for his skillful assistance in immunohistochemistry experiments. We acknowledge Dr. Michael McDermott (Department of Histopathology, Our Lady's Children's Hospital, Dublin, Ireland) for providing MPS-I lung tissue samples.

Appendix A. Supplementary data

Supplementary data to this article can be found online at https://doi.org/10.1016/j.carbpol.2022.119734.

References

Abboud-Jarrous, G., Atzmon, R., Peretz, T., Palermo, C., Gadea, B. B., Joyce, J. A., & Vlodavsky, I. (2008). Cathepsin L is responsible for processing and activation of proheparanase through multiple cleavages of a linker segment. *The Journal of Biological Chemistry, 283*, 18167–18176. https://doi.org/10.1074/jbc.M801327200

Abrahamson, M. (1994). Cystatins. *Methods in Enzymology, 244*, 685–700.

Abrahamson, M., Alvarez-Fernandez, M., & Nathanson, C.-M. (2003). Cystatins. *Biochemical Society*, 179–199.

Abrahamson, M., Barrett, A. J., Salvesen, G., & Grubb, A. (1986). Isolation of six cysteine proteinase inhibitors from human urine. Their physicochemical and enzyme kinetic properties and concentrations in biological fluids. *The Journal of Biological Chemistry, 261*, 11282–11289.

Abrahamson, M., Ritonja, A., Brown, M. A., Grubb, A., Machleidt, W., & Barrett, A. J. (1987). Identification of the probable inhibitory reactive sites of the cysteine proteinase inhibitors human cystatin C and chicken cystatin. *The Journal of Biological Chemistry, 262*, 9688–9694.

Annaval, T., Wild, R., Crétinon, Y., Sadir, R., Vivès, R. R., & Lortat-Jacob, H. (2020). Heparan sulfate proteoglycans biosynthesis and post synthesis mechanisms combine few enzymes and few Core proteins to generate extensive structural and functional diversity. *Molecules, 25*, E4215. https://doi.org/10.3390/molecules25184215

Barrett, A. J., Kembhavi, A. A., Brown, M. A., Kirschke, H., Knight, C. G., Tamai, M., & Hanada, K. (1982). L-trans-epoxysuccinyl-leucylamido(4-guanidino)butane (E-64) and its analogues as inhibitors of cysteine proteinases including cathepsins BH and L. *Biochem. J, 201*, 189–198.

Berger, K. I., Fagondes, S. C., Giugliani, R., Hardy, K. A., Lee, K. S., McArdle, C., Scarpa, M., Tobin, M. J., Ward, S. A., & Rapoport, D. M. (2013). Respiratory and sleep disorders in mucopolysaccharidosis. *Journal of Inherited Metabolic Disease, 36*, 201–210. https://doi.org/10.1007/s10545-012-9555-1

Bieth, J. G. (1980). Pathophysiological interpretation of kinetic constants of protease inhibitors. *Bulletin Européen de Physiopathologie Respiratoire, 16*(Suppl), 183–197. https://doi.org/10.1016/b978-0-08-027379-2.50020-x

Bojarski, K. K., Sage, J., Lalmanach, G., Lecaille, F., & Samsonov, S. A. (2022). In silico and in vitro mapping of specificity patterns of glycosaminoglycans towards cysteine cathepsins B, L, K, S and V. *Journal of Molecular Graphics & Modelling, 113*, Article 108153. https://doi.org/10.1016/j.jmgm.2022.108153

Bollengier, F. (1987). Cystatin C, alias post-gamma-globulin: A marker for multiple sclerosis? *Journal of Clinical Chemistry and Clinical Biochemistry, 25*, 589–593. https://doi.org/10.1515/cclm.1987.25.9.589

Bühling, F., Waldburg, N., Reisenauer, A., Heimburg, A., Golpon, H., & Welte, T. (2004). Lysosomal cysteine proteases in the lung: Role in protein processing and immunoregulation. *The European Respiratory Journal, 23*, 620–628.

Calero, M., Pawlik, M., Soto, C., Castaño, E. M., Sigurdsson, E. M., Kumar, A., Gallo, G., Frangione, B., & Levy, E. (2001). Distinct properties of wild-type and the amyloidogenic human cystatin C variant of hereditary cerebral hemorrhage with amyloidosis, icelandic type. *Journal of Neurochemistry, 77*, 628–637. https://doi.org/10.1046/j.1471-4159.2001.00256.x

Case, D., Cerutti, D., Cheatham, T., III, Darden, T., III, Duke, R., III, Giese, T., III, Gohlke, H., III, Goetz, A., III, Greene, D., III, & Homeyer, N., III (2017). *AMBER 2017*. San Francisco, CA, USA: University of California.

Chazeirat, T., Denamur, S., Bojarski, K. K., Andrault, P.-M., Sizaret, D., Zhang, F., Saidi, A., Tardieu, M., Linhardt, R. J., Labarthe, F., Brömme, D., Samsonov, S. A., Lalmanach, G., & Lecaille, F. (2021). The abnormal accumulation of heparan sulfate in patients with mucopolysaccharidosis prevents the elastolytic activity of cathepsin V. *Carbohydrate Polymers, 253*, Article 117261. https://doi.org/10.1016/j.carbpol.2020.117261

Chu, S.-C., Wang, C.-P., Chang, Y.-H., Hsieh, Y.-S., Yang, S.-F., Su, J.-M., Yang, C.-C., & Chiou, H.-L. (2004). Increased cystatin C serum concentrations in patients with hepatic diseases of various severities. *Clinica Chimica Acta, 341*, 133–138. https://doi.org/10.1016/j.cccn.2003.11.011

Chung, S., Ma, X., Liu, Y., Lee, D., Tittiger, M., & Ponder, K. P. (2007). Effect of neonatal administration of a retroviral vector expressing α-l-iduronidase upon lysosomal storage in brain and other organs in mucopolysaccharidosis I mice. *Molecular Genetics and Metabolism, 90*, 181–192. https://doi.org/10.1016/j.ymgme.2006.08.001

Chung-Hung, T., Shun-Fa, Y., & Yu-Chao, C. (2007). The upregulation of cystatin C in oral submucous fibrosis. *Oral Oncology, 43*, 680–685. https://doi.org/10.1016/j.oraloncology.2006.08.009

Cimerman, N., Prebanda, M. T., Turk, B., Popovic, T., Dolenc, I., & Turk, V. (1999). Interaction of cystatin C variants with papain and human cathepsins B, H and L. *Journal of Enzyme Inhibition, 14*, 167–174. https://doi.org/10.3109/14756369909036552

De Pasquale, V., Moles, A., & Pavone, L. M. (2020). Cathepsins in the pathophysiology of mucopolysaccharidoses: New perspectives for therapy. *Cells, 9*, E979. https://doi.org/10.3390/cells9040979

Denamur, S., Touati, G., Debelleix, S., Damaj, L., Barth, M., Tardieu, M., Gorce, M., Broué, P., Lacombe, D., & Labarthe, F. (2022). Recommended respiratory tests are not routinely performed for mucopolysaccharidosis patients. *ERJ Open Research, 8*, 00567–02021. https://doi.org/10.1183/23120541.00567-2021

Dyer, D. P., Salanga, C. L., Volkman, B. F., Kawamura, T., & Handel, T. M. (2016). The dependence of chemokine-glycosaminoglycan interactions on chemokine oligomerization. *Glycobiology, 26*, 312–326. https://doi.org/10.1093/glycob/cwv100

Ester, M., Kriegel, H.-P., Sander, J., & Xu, X. (1996). In *A density-based algorithm for discovering clusters in large spatial databases with noise* (pp. 226–231). Kdd.

Grubb, A. (2010). Non-invasive estimation of glomerular filtration rate (GFR). The Lund model: Simultaneous use of cystatin C- and creatinine-based GFR-prediction equations, clinical data and an internal quality check. *Scandinavian Journal of Clinical and Laboratory Investigation, 70*, 65–70. https://doi.org/10.3109/00365511003642535

Gupta, S., O'Meara, A., Wynn, R., & McDermott, M. (2013). Fatal and unanticipated cardiorespiratory disease in a two-year-old child with hurler syndrome following successful stem cell transplant. *JIMD Reports, 10*, 1–5. https://doi.org/10.1007/8904_2013_213

Haskins, M. E., Otis, E. J., Hayden, J. E., Jezyk, P. F., & Stramm, L. (1992). Hepatic storage of glycosaminoglycans in feline and canine models of mucopolysaccharidoses I, VI, and VII. *Veterinary Pathology, 29*, 112–119. https://doi.org/10.1177/030098589202900203

Higgins, W. J., Fox, D. M., Kowalski, P. S., Nielsen, J. E., & Worrall, D. M. (2010). Heparin enhances serpin inhibition of the cysteine protease cathepsin L. *The Journal of Biological Chemistry, 285*, 3722–3729. https://doi.org/10.1074/jbc.M109.037358

Hileman, R. E., Smith, A. E., Toida, T., & Linhardt, R. J. (1997). Preparation and structure of heparin lyase-derived heparan sulfate oligosaccharides. *Glycobiology, 7*, 231–239. https://doi.org/10.1093/glycob/7.2.231

Hoste, L., Martens, F., Cooreman, S., Doubel, P., & Pottel, H. (2014). Does the type of creatinine assay affect creatinine clearance determination? *Scandinavian Journal of Clinical and Laboratory Investigation, 74*, 392–398. https://doi.org/10.3109/00365513.2014.900186

Humphrey, W., Dalke, A., & Schulten, K. (1996). VMD: Visual molecular dynamics. *Journal of Molecular Graphics, 14*(33–38), 27–28. https://doi.org/10.1016/0263-7855(96)00018-5

Jurczak, P., Groves, P., Szymanska, A., & Rodziewicz-Motowidlo, S. (2016). Human cystatin C monomer, dimer, oligomer, and amyloid structures are related to health and disease. *FEBS Letters, 590*, 4192–4201. https://doi.org/10.1002/1873-3468.12463

Kar, S., Paglialunga, S., & Islam, R. (2018). Cystatin C is a more reliable biomarker for determining eGFR to support drug development studies. *Journal of Clinical Pharmacology, 58*, 1239–1247. https://doi.org/10.1002/jcph.1132

Kasabova, M., Joulin-Giet, A., Lecaille, F., Gilmore, B. F., Marchand-Adam, S., Saidi, A., & Lalmanach, G. (2014). Regulation of TGF-β1-driven differentiation of human lung fibroblasts: Emerging roles of cathepsin B and cystatin C. *The Journal of Biological Chemistry, 289*, 16239–16251. https://doi.org/10.1074/jbc.M113.542407

Kasabova, M., Joulin-Giet, A., Lecaille, F., Saidi, A., Marchand-Adam, S., & Lalmanach, G. (2014). Human cystatin C: A new biomarker of idiopathic pulmonary fibrosis? *Proteomics clinAppl, 8*, 447–453.

Kasabova, M., Saidi, A., Naudin, C., Sage, J., Lecaille, F., & Lalmanach, G. (2011). Cysteine cathepsins: Markers and therapy targets in lung disorders. *Clinical Reviews in Bone and Mineral Metabolism, 9*, 148–161.

Kasabova, M., Villeret, B., Gombault, A., Lecaille, F., Reinheckel, T., Marchand-Adam, S., Couillin, I., & Lalmanach, G. (2016). Discordance in cathepsin B and cystatin C expressions in bronchoalveolar fluids between murine bleomycin-induced fibrosis and human idiopathic fibrosis. *Respiratory Research, 17*, 118. https://doi.org/10.1186/s12931-016-0432-6

Kirschner, K. N., Yongye, A. B., Tschampel, S. M., González-Outeiriño, J., Daniels, C. R., Foley, B. L., & Woods, R. J. (2008). GLYCAM06: A generalizable biomolecular force field. *Carbohydrates. Journal of Computational Chemistry, 29*, 622–655. https://doi.org/10.1002/jcc.20820

Kolodziejczyk, R., Michalska, K., Hernandez-Santoyo, A., Wahlbom, M., Grubb, A., & Jaskolski, M. (2010). Crystal structure of human cystatin C stabilized against amyloid formation. *The FEBS Journal, 277*, 1726–1737. https://doi.org/10.1111/j.1742-4658.2010.07596.x

Lalmanach, G., Diot, E., Godat, E., Lecaille, F., & Hervé-Grépinet, V. (2006). Cysteine cathepsins and caspases in silicosis. *Biological Chemistry, 387*, 863–870. https://doi.org/10.1515/BC.2006.109

Lalmanach, G., Kasabova-Arjomand, M., Lecaille, F., & Saidi, A. (2021). Cystatin M/E (Cystatin 6): A janus-faced cysteine protease inhibitor with both tumor-suppressing and tumor-promoting functions. *Cancers (Basel), 13*, 1877. https://doi.org/10.3390/cancers13081877

Lalmanach, G., Saidi, A., Marchand-Adam, S., Lecaille, F., & Kasabova, M. (2015). Cysteine cathepsins and cystatins: From ancillary tasks to prominent status in lung diseases. *Biological Chemistry, 396*, 111–130. https://doi.org/10.1515/hsz-2014-0210

Lecaille, F., Brömme, D., & Lalmanach, G. (2008). Biochemical properties and regulation of cathepsin K activity. *Biochimie, 90*, 208–226. https://doi.org/10.1016/j.biochi.2007.08.011

Lecaille, F., Kaleta, J., & Brömme, D. (2002). Human and parasitic papain-like cysteine proteases: Their role in physiology and pathology and recent developments in inhibitor design. *Chemical Reviews, 102*, 4459–4488. https://doi.org/10.1021/cr0101656

Li, Z., Hou, W. S., & Brömme, D. (2000). Collagenolytic activity of cathepsin K is specifically modulated by cartilage-resident chondroitin sulfates. *Biochemistry, 39*, 529–536. https://doi.org/10.1021/bi992251u

Machleidt, W., Thiele, U., Laber, B., Assfalg-Machleidt, I., Esterl, A., Wiegand, G., Kos, J., Turk, V., & Bode, W. (1989). Mechanism of inhibition of papain by chicken egg white cystatin. Inhibition constants of N-terminally truncated forms and cyanogen bromide fragments of the inhibitor. *FEBS Letters, 243*, 234–238. https://doi.org/10.1016/0014-5793(89)80135-8

Mason, R. W., Sol-Church, K., & Abrahamson, M. (1998). Amino acid substitutions in the N-terminal segment of cystatin C create selective protein inhibitors of lysosomal cysteine proteinases. *Biochemical Journal, 330*, 833–838.

Maszota-Zieleniak, M., Danielsson, A., & Samsonov, S. A. (2021). The potential role of glycosaminoglycans in serum amyloid a fibril formation by in silico approaches. *Matrix Biol Plus, 12*, Article 100080. https://doi.org/10.1016/j.mbplus.2021.100080

Morris, G. M., Goodsell, D. S., Halliday, R. S., Huey, R., Hart, W. E., Belew, R. K., & Olson, A. J. (1998). Automated docking using a Lamarckian genetic algorithm and an empirical binding free energy function. *Journal of Computational Chemistry, 19*, 1639–1662.

Muenzer, J. (2011). Overview of the mucopolysaccharidoses. *Rheumatology (Oxford), 50* (Suppl. 5), v4–v12. https://doi.org/10.1093/rheumatology/ker394

Najjam, S., Gibbs, R. V., Gordon, M. Y., & Rider, C. C. (1997). Characterization of human recombinant interleukin 2 binding to heparin and heparan sulfate using an ELISA approach. *Cytokine, 9*, 1013–1022. https://doi.org/10.1006/cyto.1997.0246

Naudin, C., Lecaille, F., Chowdhury, S., Krupa, J. C., Purisima, E., Mort, J. S., & Lalmanach, G. (2010). The occluding loop of cathepsin B prevents its effective inhibition by human kininogens. *Journal of Molecular Biology, 400*, 1022–1035. https://doi.org/10.1016/j.jmb.2010.06.006

Nguyen, H., Maier, J., Huang, H., Perrone, V., & Simmerling, C. (2014). Folding simulations for proteins with diverse topologies are accessible in days with a physics-based force field and implicit solvent. *Journal of the American Chemical Society, 136*, 13959–13962. https://doi.org/10.1021/ja5032776

Novinec, M., Lenarčič, B., & Turk, B. (2014). Cysteine cathepsin activity regulation by glycosaminoglycans. *BioMed Research International, 2014*, Article 309718. https://doi.org/10.1155/2014/309718

Onufriev, A., Case, D. A., & Bashford, D. (2002). Effective born radii in the generalized born approximation: The importance of being perfect. *Journal of Computational Chemistry, 23*, 1297–1304. https://doi.org/10.1002/jcc.10126

Orosz, F., & Ovádi, J. (2002). A simple method for the determination of dissociation constants by displacement ELISA. *Journal of Immunological Methods, 270*, 155–162. https://doi.org/10.1016/s0022-1759(02)00295-8

Perlenfein, T. J., Mehlhoff, J. D., & Murphy, R. M. (2017). Insights into the mechanism of cystatin C oligomer and amyloid formation and its interaction with β-amyloid. *The Journal of Biological Chemistry, 292*, 11485–11498. https://doi.org/10.1074/jbc.M117.786558

Pichert, A., Schlorke, D., Franz, S., & Arnhold, J. (2012). Functional aspects of the interaction between interleukin-8 and sulfated glycosaminoglycans. *Biomatter, 2*, 142–148. https://doi.org/10.4161/biom.21316

Popović, T., Brzin, J., Ritonja, A., & Turk, V. (1990). Different forms of human cystatin C. *Biological Chemistry Hoppe-Seyler, 371*, 575–580. https://doi.org/10.1515/bchm3.1990.371.2.575

Popovic, T., Cimerman, N., Dolenc, I., Ritonja, A., & Brzin, J. (1999). Cathepsin L is capable of truncating cystatin C of 11 N-terminal amino acids. *FEBS Letters, 455*, 92–96. https://doi.org/10.1016/s0014-5793(99)00824-8

Rein, C. M., Desai, U. R., & Church, F. C. (2011). Serpin-glycosaminoglycan interactions. *Methods in Enzymology, 501*, 105–137. https://doi.org/10.1016/B978-0-12-385950-1.00007-9

Rider, C. C., & Mulloy, B. (2017). Heparin, heparan sulphate and the TGF-β cytokine superfamily. *Molecules, 22*, E713. https://doi.org/10.3390/molecules22050713

Ruiz-Gómez, G., Vogel, S., Möller, S., Pisabarro, M. T., & Hempel, U. (2019). Glycosaminoglycans influence enzyme activity of MMP2 and MMP2/TIMP3 complex formation - insights at cellular and molecular level. *Scientific Reports, 9*, 4905. https://doi.org/10.1038/s41598-019-41355-2

Samsonov, S. A., Bichmann, L., & Pisabarro, M. T. (2015). Coarse-grained model of glycosaminoglycans. *Journal of Chemical Information and Modeling, 55*, 114–124. https://doi.org/10.1021/ci500669w

Schiffl, H., & Lang, S. M. (2012). Update on biomarkers of acute kidney injury: Moving closer to clinical impact? *Molecular Diagnosis & Therapy, 16*, 199–207. https://doi.org/10.1007/BF03262209

Schwartz, G. J., & Work, D. F. (2009). Measurement and estimation of GFR in children and adolescents. *Clinical Journal of the American Society of Nephrology, 4*, 1832–1843. https://doi.org/10.2215/CJN.01640309

Shi, D., Sheng, A., & Chi, L. (2021). Glycosaminoglycan-protein interactions and their roles in human disease. *Frontiers in Molecular Biosciences, 8*, Article 639666. https://doi.org/10.3389/fmolb.2021.639666

Solem, M., Rawson, C., Lindburg, K., & Barnes, D. (1990). Transforming growth factor beta regulates cystatin C in serum-free mouse embryo (SFME) cells. *Biochemical and Biophysical Research Communications, 172*, 945–951. https://doi.org/10.1016/0006-291x(90)90767-h

Takeuchi, M., Fukuda, Y., Nakano, I., Katano, Y., & Hayakawa, T. (2001). Elevation of serum cystatin C concentrations in patients with chronic liver disease. *European Journal of Gastroenterology & Hepatology, 13*, 951–955. https://doi.org/10.1097/00042737-200108000-00013

Tocchi, A., & Parks, W. C. (2013). Functional interactions between matrix metalloproteinases and glycosaminoglycans. *The FEBS Journal, 280*, 2332–2341. https://doi.org/10.1111/febs.12198

Turk, V., Stoka, V., & Turk, D. (2008). Cystatins: Biochemical and structural properties, and medical relevance. *Frontiers in Bioscience, 13*, 5406–5420. https://doi.org/10.2741/3089

Vallet, S. D., Berthollier, C., & Ricard-Blum, S. (2022). The glycosaminoglycan interactome 2.0. *American Journal of Physiology. Cell Physiology*. https://doi.org/10.1152/ajpcell.00095.2022

Wang, J., Wang, W., Kollman, P. A., & Case, D. A. (2006). Automatic atom type and bond type perception in molecular mechanical calculations. *Journal of Molecular Graphics & Modelling, 25*, 247–260. https://doi.org/10.1016/j.jmgm.2005.12.005

Yano, S., Li, C., & Pavlova, Z. (2013). The transforming growth factor-Beta signaling pathway involvement in cardiovascular lesions in mucopolysaccharidosis-I. *JIMD Reports, 7*, 55–58. https://doi.org/10.1007/8904_2012_141

Zhang, X., Liu, X., Su, G., Li, M., Liu, J., Wang, C., & Xu, D. (2021). pH-dependent and dynamic interactions of cystatin C with heparan sulfate. *Communications Biology, 4*, 198. https://doi.org/10.1038/s42003-021-01737-7

Zhou, J., Lin, J., Leung, W. T., & Wang, L. (2020). A basic understanding of mucopolysaccharidosis: Incidence, clinical features, diagnosis, and management. *Intractable Rare Dis Res, 9*, 1–9. https://doi.org/10.5582/irdr.2020.01011